Ammonia-Assisted Fabrication of Flowery Nanostructures of Metallic Nickel Assembled from Hexagonal Platelets

Xiaomin Ni,*[a,b] Huagui Zheng,[b] Qing Yang,[b] Kaibin Tang,[b] and Guangxuan Liao[a]

A simple one-pot solution method was reported for the synthesis of metallic nickel nanostructures assembled from hexagonal nanoplatelets. The process involved the reduction of nickelous salt with hydrazine in ammonia solution, and the reaction proceeded without the use of surfactants or external magnetic forces. By properly adjusting the experimental parameters, we realized the anisotropic growth of face-centered-cubic (fcc) nickel into hexagonal nanoplatelets and

their simultaneous assembly into flowery architectures. The cooperative effects of the ammonia complexing agent, a proper reaction rate, inherent magnetic interactions, and assembly entropy were considered the key factors driving the formation of the special assembly nanostructures on the basis of a series of contrast experiments.
(© Wiley-VCH Verlag GmbH & Co. KGaA, 69451 Weinheim, Germany, 2009)

Introduction

Metal nanoparticles with various shapes and organizations have been of great interest in material synthesis for their relevance to the construction of nanodevices.[1] Among them, magnetic metal assemblies are paid particular attention for their novel properties, which are different from their isolated or bulk counterparts, and for their wide potential applications in catalysis, drug delivery, conduction, magnetic recording, biological labeling, and electron devices.[2–5] Metallic nickel, as one of the most used elements, shows applications spanning over almost all sizes and fields.[6–8] Its uses today and in the future would benefit from materials designed with nanosized novel morphologies.[9] Most nickel assembly nanostructures are fabricated by two methods. One method involves harnessing the noncovalent interactions between the organic molecules functionalized nanoparticles, including van der Waals forces, π–π interactions, electrostatic forces, and hydrogen bonding, which act as the "mortar" to associate the building blocks into certain configurations.[10,11] For example, nickel nanoparticles modified with C12SH formed an ordered assembly through attractive van der Waals interactions between the hydrophobic outer face of the nickel subunits.[12] Nickel nanorods covered with hexadecylamine spontaneously organized into aggregates with their long axes parallel to each other.[13] However, in these assemblies, the content of or-

ganic molecules was relatively high, which usually damaged their magnetic properties.[14] When immersed into some solvents, dissolution of the "mortar" made the assembly collapse, which resulted in difficulty in their applications as nanodevices.[12,13] Another efficient method to build nickel assembly nanostructures is by the direction of magnetic field, which typically produces 1D chains of particles with the magnetic dipoles aligned head-to-tail and parallel to the magnetic field.[15–17] For instance, colloidal nickel nanoparticles self-assembled into nanochains when subjected to a magnetic field with a strength of about 250 Gauss.[18] 1D microwires assembled from nickel nanoneedles were fabricated in the presence of an external magnetic field of 0.2 T.[19] Hierarchical nanowires and nanoflowers were fabricated by a nonaqueous sol–gel approach in static constant and rotating magnetic fields, respectively.[20] However, these assemblies usually required an external magnetic field to remain stable, and when the external magnetic field was removed from the system, the alignments destabilized.[21,22] As a result, additional equipment is needed to sustain the assembled nanostructure, which sometimes makes the preparation inconvenient. Nowadays, the development of simple approaches for multidimensional interconnection of nanoscaled building blocks into desired structures is still a significant challenge for material scientists. Recently, we reported the fabrication of a series of assembly nickel nanostructures without any surfactants or external magnetic field.[23–25] The present work, as a continuation of our research endeavor in this area, reports another simple and time-saving method for the synthesis of a new type of nickel assembly nanostructures independent of any surfactants or external magnetic forces. The process involves the reduction of nickelous salt with hydrazine in ammonia solution within 4 h. By properly adjusting the experimental parameters, we

_____

[a] State Key Laboratory of Fire Science, University of Science and Technology of China, Hefei,
Anhui 230026, P. R. China
Fax: +86-551-3601669
E-mail: nxmin@ustc.edu.cn
[b] Department of Chemistry, University of Science and Technology of China,
Hefei, Anhui 230026, P. R. China

realized the anisotropic growth of face-centered-cubic (fcc) nickel into hexagonal nanoplatelets and their simultaneous assembly into flowery architectures.

Results and Discussion

Morphological and Structural Characterization

As shown in Figure 1, the typical morphology of the as-prepared nickel sample was flowery crystallite with a size of 5–15 µm. Each flower exhibited a hierarchical structure, which consisted of columnar petals radiating from the center. All the constituent columns were assembled by dozens of hexagonal platelets stacking in a face-to-face fashion. Interestingly, it was found that the platelet subunits were crossbedded self-adhesive. The platelets had a side length of 0.2–1 µm and a thickness of 50–100 nm. Such assembling characteristics are also reflected in the corresponding TEM image of Figure 1f, in which the flakes are viewed edgewise. A typical isolated hexagonal platelet displayed in Figure 1g showed a side length of about 1 µm and an angle between the two adjacent edges of 120°. The corresponding SAED pattern could be indexed to fcc nickel with the electron beam along the [111] zone direction. The six spots nearest the center spot could be indexed to $1/3[\bar{4}22]$ diffractions of fcc nickel, whereas the spots located further away were due to the (220) lattice planes of a fcc single crystal. Emergence of $1/3[\bar{4}22]$ forbidden diffractions in the [111] zone spots could be ascribed to structural defects, such as stacking faults in the [111] axis, which was similar to that observed in thin Au or Ag crystals.[26–28] The HRTEM image of the platelet showed a 2D lattice with a spacing of 2.16 Å, which is in accord with the separation between the $1/3[\bar{4}22]$ planes of fcc Ni. This was in good agreement with a fcc single crystal oriented along the [111] direction, indicating the platelet was a single crystalline structure with the up and bottom faces of (111) planes. Thus, the side faces of the platelets could be ascertained as (110) planes of fcc Ni. The assembling manner of each columnar petal of the flowery architecture is schematically shown in Scheme 1.
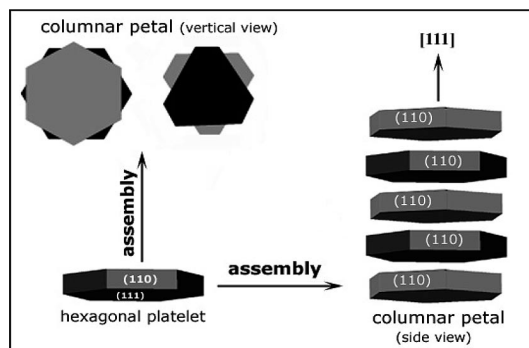
Scheme 1. Schematic illustration of the assembly of the hexagonal nanoplatelets.

Evolution Process of the Nanoflowers

In order to investigate the formation process of the novel flowers, time-dependent evolution of the product was observed through XRD and SEM. It was found that the initial product of the reaction was β-Ni(OH)$_2$ and not metallic nickel, as revealed by the XRD patterns of Figure 2a. After the starting solution was heated for 0.5 h, the supernatant solution became colorless and precipitation of green β-Ni(OH)$_2$ powder was observed. Dimethylglyoxime tests indicated that nearly all soluble Ni^{II} species had transformed into solid nickel hydroxides. With the reaction processed, the content of β-Ni(OH)$_2$ decreased and metallic nickel gradually predominated the product (Figure 2b,c). When the reaction time was prolonged to 4 h, hydroxide disappeared and the product became pure metallic fcc nickel (Figure 2d). We collected the products at different stages, separated the metallic nickel and the hydroxide apart by magnetic decantation, and then studied their morphologies, respectively.

The SEM images in Figure 3 indicate that the initial nickel product consisted of coarse spheres, which were assembled from nanoparticles with a diameter of 50 nm (Figure 3a). At the second stage, hexagonal platelets grew out around the surface of the spherical aggregate and spontaneously arranged with the top/bottom faces oriented the same, as seen in Figure 3b. These hexagonal nanoplatelets gradually stacked face-to-face and finally developed into
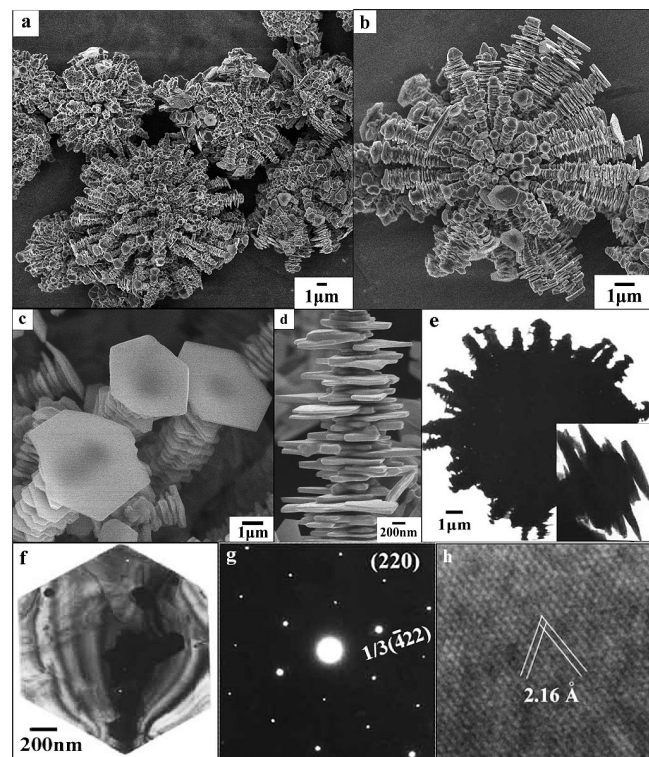

Figure 1. SEM images of the obtained nickel sample: (a) a panoramic image, (b) a typical flowery structure, (c) magnified image of the flowery petals, (d) magnified image of the tops of the petals, (e) TEM image of an individual flower; inset was part of the columnar petal, (f) TEM image of a typical hexagonal platelet unit, (g) the corresponding SAED pattern, (h) HRTEM image of the platelet.
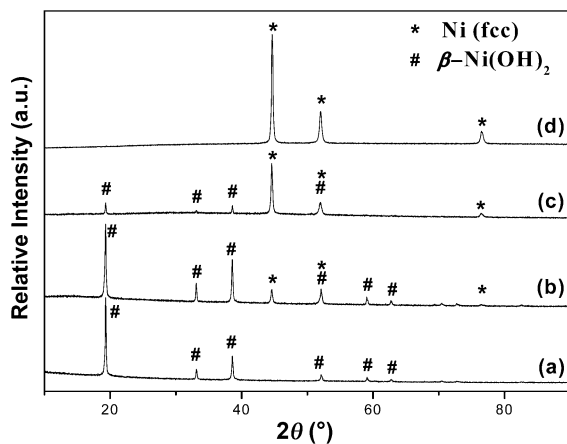
Figure 2. XRD patterns of the product obtained at different reaction stages: (a) 0.5 h, (b) 1.0 h, (c) 3.0 h, (d) 4.0 h.

columnar petals that are radially located on the initial spherical cores (Figure 3c). In contrast, we observed that the β-Ni(OH)$_2$ rudiments were pancake-shaped, which were formed through the stacking of nanosheets (Figure 3d). With the reaction processed, these crystallites with defined shapes gradually broke into irregular fragments, as shown in Figure 3e,f.
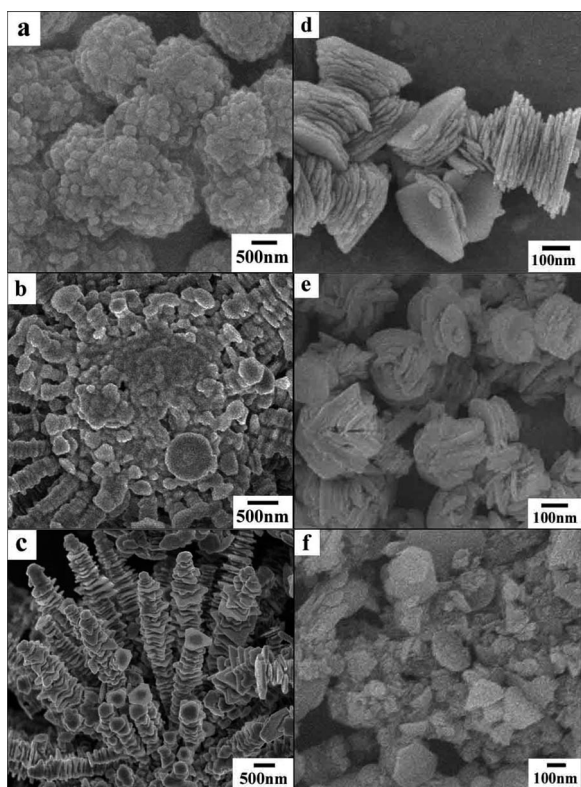

Figure 3. (a), (b), and (c) SEM images of the metallic nickel separated from the system at reaction stages of 1.0, 3.0, and 4.0 h, respectively. (d), (e), and (f) SEM images of the β-Ni(OH)$_2$ product separated from the system at reaction stages of 0.5, 1.0, and 3.0 h, respectively.

Effect of the Experimental Conditions on the Product Morphologies

It was found that the molar ratio (ω) between ammonia and hydrazine plays an important role in controlling the morphology of the final product. Figure 4 shows the typical SEM images of the three samples prepared at different ω values. Without ammonia, the product emerged as irregular particles, whereas pearl chain-like microwires were produced at values of ω above 12. When the ω value was increased to 20, large coarse crystallites were produced, as seen in Figure 4c. The optimized ω value suitable for the formation of the flowery architectures was between 6 and 10. In the system, ammonia was introduced as the complexing agent and the source of hydroxide ions. The ammonia molecules coordinated with the Ni^{2+} ions to form a Ni(NH$_3$)$_6$$^{2+}$ complex; formation of this complex decreased the amount of free Ni^{2+} ions in solution, which resulted in a relatively slow reaction rate. In addition to the small amount of ammonia molecules as the complexing agent, the excessive amount of ammonia in the solution partly ionized and released the hydroxide ions, which inevitably resulted in the reduction of Ni^{2+} to metallic Ni by hydrazine. It is known that the reducing power of hydrazine increases with the basicity of the medium. A proper concentration of ammonia was found to effectively control the reducing power of hydrazine by yielding a suitable concentration of hydroxides ions, and thus, the reaction rate and growth rate of the nickel platelets and their spontaneous assembly into flowers was kinetically modulated.
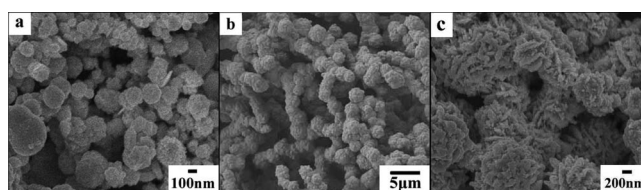

Figure 4. SEM images of the samples prepared in the systems with different molar ratios (ω) of ammonia to hydrazine: (a) ω = 0, (b) ω = 12, (c) ω = 18.

Temperature also showed a significant influence on the product morphology. Keeping the other reaction conditions constant, the optimized temperature for the production of the nickel flowers was 100–140 °C. At a temperature lower than 100 °C, the product was made up of microcrystallites, which were assembled from branched and interconnected
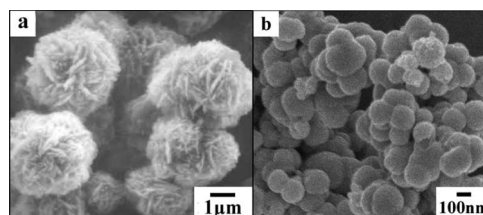

Figure 5. SEM images of the samples prepared at a temperature of (a) 100 °C and (b)160 °C.

nanosheets (Figure 5a). When the temperature increased above 140 °C, the product became spherical particles, possibly for a faster reaction rate (Figure 5b).

Possible Formation Mechanism

The formation of magnetically assembled nanostructures was a complex process that was influenced by several factors, such as the reaction velocity, shape of the building blocks, spatial hindrance, magnetic interactions, and so on.[29] On the basis of the above experimental results, we proposed that the configuration of the flower-like nickel nanostructure assemblies could be ascribed to the cooperative effect of the ammonia complexing agent, kinetic control, inherent magnetic interactions, and assembly entropy. In the system, ammonia molecules were considered to have a threefold purpose: to serve as the complexing agent, to serve as the source of hydroxide ions, and to serve as the structure-directing agent. When the solution was heated, decomplexation of $Ni(NH_3)_6^{2+}$ occurred first for its higher reaction rate than the redox reaction, resulting in the precipitation of β-$Ni(OH)_2$ from the solution. Then, these newly formed hydroxide ions dissociated in solution and released free Ni^{2+} ions. The free Ni^{2+} ions were reduced by hydrazine to metallic Ni, which could be described as a solid–solution–solid process.[30,31] Because the solubility of nickel hydroxide was low, the concentration of Ni^{2+} in solution was also correspondingly low. Therefore, the reduction rate and crystal growth rate were relatively slow, which may be favorable for the anisotropic growth of nickel nanocrystals. Here, it was found that the special-shaped hydroxide was crucial for the formation of the unique nickel nanostructures. Keeping the other conditions constant, replacement of the hydroxide initial stacking platelets with other-shaped counterparts such as flowers, hexagonal platelets, or particulates did not result in such hierarchical nickel nanostructures (Figure 6). It was possibly the different solubility of these hydroxide ions that led to unfavorable reaction rates for the growth of the nickel flowers.[31] Second, ammonia was also considered to play the role of structure-directing agent, which modulated the orientation growth of nickel nanocrystals into hexagonal platelets. In a contrasting experiment, the tower-shaped hydroxide ions (as shown in Figure 3d) were reduced in a system without ammonia and the results showed that only spherical nickel crystallites could be fabricated. this experiment revealed the important effect of ammonia on the anisotropic growth of nickel nanocrystals. During the crystal growth process, ammonia molecules may selectively absorb on the (111) planes of the fcc nickel for the affinity between nickel and ammonia.[32] Thus, the growth rates of different crystalline planes were kinetically adjusted, in which the (111) planes were passivated, while the (110) planes were seldomly affected. As a result, the nickel crystals developed into hexagonal plates with the top/bottom faces of (111) planes. In contrast, we noted that these platelets all aligned with (111) planes oriented the same. It was known that the [111] direction was

the magnetic easy axis of fcc nickel.[33] Such an assembling manner with the magnetic easy axis oriented the same facilitated the reduction of magnetic anisotropic energy.[19] At the same time, for the hexagonal platelets, such a face-to-face packing mode can maximize the entropy of the self-assembled structures by minimizing the excluded volume per nanoplatelet in the array through the existence of a nematic phase.[34] Therefore, the magnetic interactions and the assembly entropy may be an inherent driving force for the assembly of the nickel platelets.
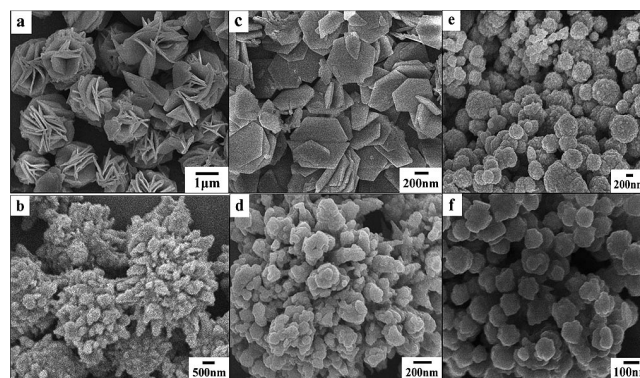

Figure 6. SEM images of the nickel samples prepared from differently shaped β-$Ni(OH)_2$ precursors: (a) β-$Ni(OH)_2$ flowers and (b) their reduced product of nickel; (c) hexagonal platelets of β-$Ni(OH)_2$ and (d) their reduced product of nickel; (e) spherical β-$Ni(OH)_2$ particles and (f) their reduced product of nickel.

In our previous work, another kind of assembly nickel nanostructure with similar morphology was prepared in the system with dimethylglyoxime (dmg) as the complexing agent instead of ammonia, but the size was much smaller (about 1 μm) and the packing of the platelets were overlapped not crossbedded.[25] It was found that the two reaction systems both underwent a solid–solution–solid process, but the reaction rate was much different. The similar morphology was possible due to the similar reaction process, in which dmgH and ammonia both acted as the complexing agent and structure-directing agent with the same coordinating nitrogen atom except that ammonia played the additional role of alkali source. However, the different product sizes may be ascribed to the different reaction rates. In the former system, the initial solid $Ni(dmg)_2$ precursor was only 2.8×10^{-5} mol with a solubility product (K_{sp}) of 4.5×10^{-24}, which resulted in a slow release rate of Ni^{2+} and a long reduction process of 12 h.[35] However, in the present system with 1.0×10^{-3} mol of $Ni(OH)_2$ ($K_{sp} = 2.5 \times 10^{-15}$) as the solid precursor, the reaction proceeded at a much faster rate and was complete in 4 h.[36] The higher concentration of the reactants and the faster reaction rate produced a larger amount of nickel atoms at the same time, which resulted in relatively large-sized building blocks and the final assembly structures. As to the crossbedded packing of the platelets in this case, it could be ascribed to the fact that such a stacking mode could further decrease the magnetic interactions between the neighboring subunits with a relatively large size by reducing the overlapping surface area.

Scheme 2 illustrates a possible formation process of the flowers. At the initial reaction stage, nickel nanoparticles were produced and they spontaneously aggregated together into spheres to lower the surface energy. Then, under the confinement of ammonia molecules, these surface particles gradually developed into hexagonal platelets. As the reaction progressed, more nickel platelets were reduced and the newly produced nickel platelets could spontaneously attach onto the formerly formed one with their similarly oriented axes to reach a low magnetic anisotropy energy. This process was repeated and the columnar petals grew longer until all the hydroxide ions were consumed, which eventually resulted in flower-like nickel nanostructure assemblies. During the whole reaction process, a suitable reaction rate was crucial for the growth of the hexagonal platelets and their spontaneous assembly. Only by proper monitoring of the reaction conditions, such as the concentration of ammonia and the temperature, could the formation of hexagonal platelets and their subsequent oriented organization be realized. Further research is needed to probe the actual mechanism of formation of the flowers and the corresponding work is underway.
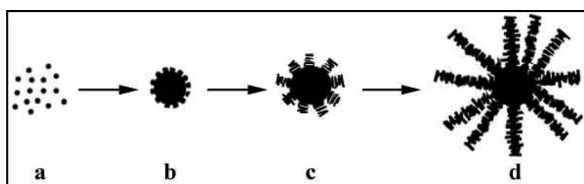
Scheme 2. Schematic illustration of the possible formation process of the flower-like, assembled nanostructure of nickel: (a) small nickel nucleus, (b) the nucleus aggregated into a sphere, (c) hexagonal platelets developed from the sphere surface, (d) more platelets stacked on the core sphere with the (111) planes oriented in the same direction.

Magnetic Properties

The magnetic properties of nanomaterials are highly dependent on their size, shape, crystallinity, magnetization orientation, and so on. Magnetic properties of the flowery architectures were measured at room temperature, which exhibited a coercivity (H_c) of 274 Oe, a saturation magnetism (M_s) of 44.8 emu g^{-1}, and a remanent magnetism (M_r) of 9.6 emu g^{-1}. In comparison to bulk nickel, the coercivity was greatly enhanced, possibly as a result of the nanosize.[37,38] Such an H_c value was also superior to that of the counterparts prepared from the dmgH system and nonaqueous sol–gel approach, which was believed to be associated with the unique packing manner of the singly crystalline nanoplatelets in the hierarchical nanostructures.[20,25] This value, however, was much lower than that of the 1D nanorods (332 Oe) or nanobelts (640 Oe), which might be due to the fact that the flowery configuration as a total exhibited a much lower anisotropy than isolated 1D nanocrystals.[39,40] When subjected to an external magnetic field, it was difficult for the radially orientated petals to be aligned simultaneously along the direction of the magnetic field like isolated nanorods or wires. Therefore, a relatively

lower H_c value was shown. As for the decreased M_s value, it might likewise be due to the decrease in the particle size accompanied by an increase in the surface area, and the magnetic interaction between the subunits, which reduced the total magnetic moment at a given field.[41–43]

Conclusions

In summary, a facile solution method was developed for the fabrication of novel hierarchical nickel nanostructures that are assembled by hexagonal nanoplatelets without the assistance of any surfactants or external magnetic forces. The structure, magnetic properties, and possible mechanism of formation of the flowery structures were studied. It was found that the ammonia complexing agent, the concentration of the reagent, the inherent dipole–dipole interactions, and the assembly entropy played important roles in the formation of the nickel flower assembly. The present work provided a simple kinetic-control route for the synthesis of magnetic assembly architectures by properly adjusting the reaction conditions, which could be extended to the fabrication of other magnetic assemblies with interesting and complex configurations. The special nickel assembly nanostructures are expected to find applications in the fields of catalysis, electron conduction, and so forth.

Experimental Section

All chemicals used were of analytical grade. In a typical synthesis, $NiCl_2 \cdot 6H_2O$ (1.0 mmol) was dissolved in diluted ammonia solution (39 mL) to give a blue transparent solution. Then, hydrazine hydrate ($N_2H_4 \cdot H_2O$; 85% w/w, 1.0 mL) was added. The mixture was transferred to a 45-mL Teflon-lined autoclave and the temperature was maintained at 120 °C for 4 h. The resulting black powder was collected, washed, and finally dried in vacuo at 50 °C for 4 h.

X-ray diffraction (XRD) patterns of the samples were recorded with a Philips X′pert diffractometer with Cu-K_α radiation (λ = 1.54178 Å). The morphology and structure of the samples were studied with transmission electron microscopy (TEM, Hitachi, H-800) with an accelerating voltage of 200 kV, and field emission scanning electron microscopy (FE-SEM, JEOL JSM-6300F). High-resolution transmission electron microscopy (HRTEM) images and the selected area electron diffraction (SAED) pattern were recorded with a JEOL-2010 TEM at an acceleration voltage of 200 kV. M-H hysteresis loops (Figure 7) were recorded on a vibrating sample magnetometer (BHV-55).
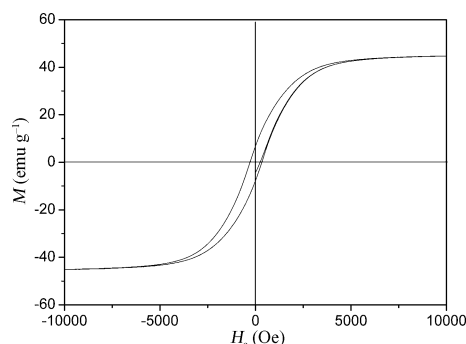

Figure 7. M-H hysteresis loop of the resulting nickel flowers.

Acknowledgments

[1] S. H. Sun, C. B. Murray, D. Weller, L. Folks, A. Moser, *Science* **2000**, *287*, 1989–1992.
[2] B. Z. Tang, Y. H. Geng, J. W. Y. Lam, B. S. Li, X. B. Jing, X. H. Wang, F. S. Wang, A. B. Pakhomov, X. X. Zhang, *Chem. Mater.* **1999**, *11*, 1581–1589.
[3] M. Kryszewski, J. K. Jeszka, *Synth. Met.* **1998**, *94*, 99–104.
[4] V. F. Puntes, P. Gorostiza, D. M. Aruguete, N. G. Bastus, A. P. Alivisatos, *Nat. Mater.* **2004**, *3*, 263–268.
[5] M. Bruchez, M. Moronne, P. Gin, S. Weiss, A. P. Alivisatos, *Science* **1998**, *281*, 2013–2016.
[6] W. X. Zhang, C. B. Wang, H. L. Lien, *Catal. Today* **1998**, *40*, 387–395.
[7] R. Hernandez, S. Polizu, S. Turenne, L. Yahia, *Bio-Med. Mater. Eng.* **2002**, *12*, 37–45.
[8] A. Smogunov, A. Dal Corso, E. Tosatti, *Surf. Sci.* **2002**, *507*, 609–614.
[9] A. Ekstrand, K. Jansson, G. Westin, *J. Sol-Gel Sci. Technol.* **2000**, *19*, 353–356.
[10] R. P. Andres, J. D. Bielefeld, J. I. Henderson, D. B. Janes, V. R. Kolagunta, C. P. Kubiak, W. J. Mahoney, R. G. Osifchin, *Science* **1996**, *273*, 1690–1693.
[11] J. Jin, T. Iyoda, C. Cao, Y. Song, L. Jiang, T. J. Li, D. B. Zhu, *Angew. Chem. Int. Ed.* **2001**, *40*, 2135–2138.
[12] S. B. Lei, C. Wang, S. X. Yin, L. J. Wan, C. L. Bai, *ChemPhysChem* **2003**, *4*, 1114–1117.
[13] N. Cordente, R. M. Espaud, F. Secocq, M. J. Casanove, C. Amies, B. Chaudret, *Nano Lett.* **2001**, *1*, 565–568.
[14] J. Osuna, D. de Caro, C. Amiens, B. Chaudret, E. Snoeck, M. Respaud, J. M. Broto, A. Fert, *J. Phys. Chem.* **1996**, *100*, 14571–14574.
[15] M. Tanase, L. A. Bauer, A. Hultgren, D. M. Silevitch, L. Sun, D. H. Reich, P. C. Searson, G. J. Meyer, *Nano Lett.* **2001**, *1*, 155–158.
[16] E. V. Shevchenko, D. V. Talapin, A. L. Rogach, A. Komowski, M. Haase, H. Weller, *J. Am. Chem. Soc.* **2002**, *124*, 11480–11485.
[17] V. F. Puntes, K. M. Krishnan, A. P. Alivisatos, *Science* **2001**, *291*, 2115–2117.
[18] S. Singamaneni, V. Bliznyuk, *Appl. Phys. Lett.* **2005**, *87*, 162511–3.
[19] H. Niu, Q. Chen, M. Ning, Y. Jia, X. Wang, *J. Phys. Chem. B* **2004**, *108*, 3996–3999.
[20] F. Jia, L. Zhang, X. Shang, Y. Yang, *Adv. Mater.* **2008**, *20*.1050–1054.
[21] B. A. Grzybowski, H. A. Stone, G. M. Whitesides, *Nature* **2000**, *405*, 1033–1036.
[22] F. Assi, R. Jenks, J. Yang, C. Love, M. Prentiss, *J. Appl. Phys.* **2002**, *92*, 5584–5586.
[23] X. Ni, Q. Zhao, H. Zheng, B. Li, J. Song, D. Zhang, X. Zhang, *Eur. J. Inorg. Chem.* **2005**, *23*, 4788–4793.
[24] X. Ni, Q. Zhao, Y. Zhang, H. Zheng, *Eur. J. Inorg. Chem.* **2007**, *3*, 422–428.
[25] X. Ni, Q. Zhao, D. Zhang, X. Zhang, H. Zheng, *J. Phys. Chem. C* **2007**, *111*, 601–605.
[26] R. Jin, Y. Cao, C. A. Mirkin, K. L. Kelly, G. C. Schatz, J. G. Zheng, *Science* **2001**, *294*, 1901–1903.
[27] M. Maillard, S. Giorgion, M. P. Pileni, *Adv. Mater.* **2002**, *14*, 1084–1086.
[28] V. Germain, J. Li, D. Ingert, Z. L. Wang, M. P. Pileni, *J. Phys. Chem. B* **2003**, *107*, 8717–8720.
[29] R. J. Nikhil, *Angew. Chem. Int. Ed.* **2004**, *43*, 1536–1540.
[30] D. Ung, G. Viau, C. Ricolleau, F. Varmont, P. Gredin, F. Fiévet, *Adv. Mater.* **2005**, *17*, 338–344.
[31] Z. Wang, J. Liu, X. Chen, J. Wan, Y. Qian, *Chem. Eur. J.* **2005**, *11*, 160–163.
[32] A. Borgna, R. Fréty, M. Primet, M. Guénin, *Appl. Catal.* **1991**, *76*, 233–254.
[33] D. F. Wan, X. L. Ma, *Magnetic Physics*, Publishing House of Electronics Industry, Beijing, **1999**, p. 178.
[34] W. Du, X. Qian, X. Ma, Q. Gong, H. Cao, J. Yin, *Chem. Eur. J.* **2007**, *13*, 3241–3247.
[35] W. Chang, K. Li, *Concise Handbook of Analytic Chemistry*, 1st ed., Science Press **1980**, p. 75.
[36] W. Chang, K. Li, *Concise Handbook of Analytic Chemistry*, 1st ed., Science Press **1980**, p. 279.
[37] J. H. Hwang, V. P. Dravid, M. H. Teng, J. J. Host, B. R. Elliott, D. L. Johnson, T. O. Mason, *J. Mater. Res.* **1997**, *12*, 1076–1082.
[38] J. Bao, Y. Liang, Z. Xu, L. Si, *Adv. Mater.* **2003**, *15*, 1832–1835.
[39] Z. Liu, S. Li, Y. Yang, S. Peng, Z. Hu, Y. Qian, *Adv. Mater.* **2003**, *15*, 1946–1948.
[40] X. M. Ni, X. B. Su, Z. P. Yang, H. G. Zheng, *J. Cryst. Growth* **2003**, *252*, 612–617.
[41] K. V. P. M. Shaf, A. Gedanken, R. Prozorov, J. Balogh, *Chem. Mater.* **1998**, *10*, 3445–3450.
[42] N. Cordente, C. Amiens, B. Chaudret, M. Respaud, F. Senocq, M. J. Casanove, *J. Appl. Phys.* **2003**, *94*, 6358–6365.
[43] D. H. Chen, S. H. Wu, *Chem. Mater.* **2000**, *12*, 1354–1361.